ChemComm

RSC Publishing

COMMUNICATION

View Article Online
View Journal | View Issue

Cite this: *Chem. Commun.*, 2013, **49**, 4331

Received 10th July 2012,
Accepted 8th August 2012

DOI: 10.1039/c2cc34934e

www.rsc.org/chemcomm

Facile assembly of an efficient CoO_x water oxidation electrocatalyst from Co-containing polyoxotitanate nanocages†‡

Yi-Hsuan Lai,[a] Chia-Yu Lin,[a] Yaokang Lv,[bc] Timothy C. King,[b] Alexander Steiner,[d] Nicoleta M. Muresan,[a] Lihua Gan,[c] Dominic S. Wright*[b] and Erwin Reisner*[a]

Cobalt-containing polyoxotitanates (TiCo) are excellent precursors for the simple and scalable preparation of Nocera-type CoO_x water-oxidation electrocatalysts. The TiCo cages serve as a reservoir for cobalt ions in a titania matrix on fluoride-doped tin oxide electrodes, and form, *in situ*, the active CoO_x catalyst for O_2 evolution with high stability in phosphate buffer in pH neutral water.

The production of H_2 through electro- or photochemical water splitting is a promising approach to provide renewable energy.[1] Efficient and stable water oxidation is generally considered as the major challenge in water splitting, because it requires finely tuned proton-coupled four-electron chemistry[2] and continued exposure to highly anodic conditions.[3] Research into effective oxygen evolution catalysts is, therefore, indispensable if water splitting is to become a viable technology.

Recent examples for water oxidation systems include electrodes modified with nature's catalyst photosystem II,[4] molecular synthetic catalysts,[5] and metal oxides.[6] Cobalt-containing catalysts have emerged as a particularly efficient and affordable candidate for water splitting.[7] In water oxidation, various cobalt(II) salts (*e.g.* $Co(NO_3)_2$, $CoSO_4$, $CoCl_2$, *etc.*)[6a,8] form CoO_x in phosphate buffer (Co–P_i) *in situ* during electro-deposition on an indium–tin oxide substrate at high potential for several hours.[6a] Co–P_i shows high electroactivity toward water oxidation and self-healing features *via* a series of linked equilibria.[9] Recently, a cobalt polyoxometalate (Co–POM) complex[10] was reported to form active CoO_x films after decomposition of the Co–POM during electrocatalysis.[11]

We are interested in the application of mixed-metal nanocages as precursors for water oxidation catalysts and our current attention focuses on heterobimetallic polyoxotitanate nanocages $[Ti_xO_y(OR)_zM_n]$ (where M is a transition metal).[12] Such doped titania cages can act as readily-hydrolysable single-source precursors for the preparation of metal-doped TiO_2 films with tunable nanostructures and electro- and photochemical properties.[13] To the best of our knowledge, however, there is no report on the use of heterometallic polyoxotitanate nanocages as pre-electrocatalysts for electrochemical water oxidation.

In this communication, we report the preparation of efficient CoO_x water oxidation electrocatalysts from the nanosized TiCo cages $[Ti_{12}O_{15}(O^iPr)_{17}]^+[(CoBr)_6Ti_{15}O_{24}(O^iPr)_{18}(Br)]^-$ (**1**) and $[(CoI)Ti_{11}O_{14}(O^iPr)_{17}]$ (**2**). Cages **1** and **2** were prepared in one step by heating $Ti(O^iPr)_4$ and CoX_2 (where X is Br or I) in an approximately 9 to 1 ratio.§ The solid-state structures of the previously reported bromide cage (**1**)[14] and the novel neutral heterometallic $Ti_{11}Co$ cage (**2**) are shown in Fig. 1.¶

The ion-separated cage pair in **1** shows the notable encapsulation of a 'naked' Br^- anion at the centre of the spherical shell of the $[(CoBr)_6Ti_{15}O_{24}(O^iPr)_{18}(Br)]^-$ anion.[14] The solid-state structure

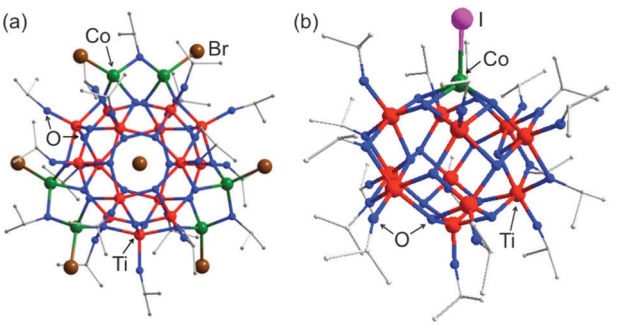

Fig. 1 (a) The cage anion of $[Ti_{12}O_{15}(O^iPr)_{17}]^+[(CoBr)_6Ti_{15}O_{24}(O^iPr)_{18}(Br)]^-$ (**1**). A full structural description and data can be found in ref. 14. (b) Crystallographic structure of the $Ti_{11}Co$ cage $[(CoI)Ti_{11}O_{14}(O^iPr)_{17}]$ (**2**) as ball and stick representation for all non-H atoms. Selected bond lengths (Å) and angles (°): Co–O_{oxo} range 1.859(14)–2.082(15), Co–I 2.589(4), Co–O 1.970(14)–2.228(16), O–Co–O range 76.2(6)–101.3(6), O–Co–I range 107.6(4)–116.4(5). Ti (red), O (blue), C (grey), Co (green), Br (brown), I (magenta).

[a] *Christian Doppler Laboratory for Sustainable SynGas Chemistry, Department of Chemistry, University of Cambridge, Lensfield Road, Cambridge CB2 1EW, UK. E-mail: reisner@ch.cam.ac.uk*
[b] *Department of Chemistry, University of Cambridge, Lensfield Road, Cambridge CB2 1EW, UK. E-mail: dsw1000@cam.ac.uk*
[c] *Department of Chemistry, Tongjii University, 1239 Siping Road, Shanghai, 200092, PR China*
[d] *Department of Chemistry, University of Liverpool, Liverpool L69 7ZD, UK*

† This article is part of the ChemComm 'Emerging Investigators 2013' themed issue.

‡ Electronic supplementary information (ESI) available: Experimental details, crystallographic data and spectral data. CCDC 891835. For ESI and crystallographic data in CIF or other electronic format see DOI: 10.1039/c2cc34934e

of **2** is similar to the cationic cage in **1**, but one of the $[TiO]^{2+}$ moieties is replaced by a $[CoI]^{+}$ unit. The Co^{II} centre of **2** adopts a highly distorted square-based pyramidal coordination geometry, with the Co–O bond lengths [1.970(14)–2.228(16) Å] and O–Co–O angles [107.6(4)–116.4(5)°] varying over a broad range. Unlike **1**, in which one of the bromide anions is located at the centre of the spherical shell, the iodide anion in **2** has a more conventional *exo*-bonding mode [Co–I 2.589(4) Å]. The reason for this difference is unclear but is most likely the result of the much greater ionic radius of I^{-} compared to Br^{-}. It can be noted in this regard that the $Ti_{11}O_{14}$ shell of **2** measures approximately 3.7 to 5.8 Å and is too small to accommodate an iodide ion. The optical and electrochemical properties of **2** are shown in Fig. S1 and S2 (ESI‡).

Electrodes for water oxidation were prepared by drop-casting fresh solutions of the TiCo nanocages **1** or **2** (40 μL of 0.01 M in dichloromethane) on fluoride-doped tin oxide (FTO, exposed area of 0.5 cm^2) coated glass. The FTO|TiCo electrodes, *i.e.*, FTO|**1** and FTO|**2**, were dried for 20 min in air at room temperature, whereupon the electrodes were rinsed with water. For comparison, FTO|$Co(NO_3)_2$ was also prepared by drop-casting $Co(NO_3)_2{\cdot}6H_2O$ (40 μL of 0.01 M in water) on FTO by the same method. The electrodes were then immersed into an electrochemical cell containing phosphate (P_i) electrolyte solution (0.1 M, pH 7). All electrochemical experiments were performed using a conventional three-electrode system with the (un)modified FTO working electrode, a Pt foil counter electrode and a Ag/AgCl/saturated KCl reference electrode at 25 °C under N_2. A stable electrode film was obtained in 5 min by cycling the electrochemical potential five times between 0.2 and 1.7 V *vs.* NHE with a scan rate of 50 mV s^{-1}.

Cyclic voltammograms (CVs) for FTO|**1**, FTO|**2**, FTO|-$Co(NO_3)_2$ and unmodified FTO electrodes in P_i solution (0.1 M and pH 7) at a scan rate of 50 mV s^{-1} are shown in Fig. 2. FTO|**1** and FTO|**2** exhibit comparable electrochemical responses with a Co^{III}/Co^{II} oxidation wave at approximately E_p = 1.20 V, followed by catalytic oxidation of water at an onset potential of approximately 1.27 V *vs.* NHE. FTO|$Co(NO_3)_2$ and unmodified FTO electrodes show less favorable electrochemical responses and high anodic currents are only observed at more positive potentials. The poor performance of FTO|$Co(NO_3)_2$ can, at least in part, be attributed to the weak attachment of the cobalt ions on the FTO surface and its removal during the rinsing procedure (Fig. 2a). In contrast, Co ions in FTO|**1** and FTO|**2** are entrapped in the Ti–O–Ti network, resulting from hydrolysis and polycondensation of the polyoxotitanate nanocages after the drop-casting procedure by moisture in air.[15]

The FTO|TiCo electrodes not only exhibited high electrocatalytic activity, but also showed high stability in a pH neutral P_i solution (Fig. 2b). An initial current density of 0.8 mA cm^{-2} at an applied potential of 1.35 V *vs.* NHE was obtained, which retained approximately 80% of the initial density after 1 h. The FTO|$Co(NO_3)_2$ electrode exhibited an initial current density of 0.52 mA cm^{-2} and approximately 80% of electroactivity was lost after 1 h. Employing the FTO|TiCo electrodes in a Na_2SO_4 (0.1 M) solution resulted in a reduced initial current response (0.55 mA cm^{-2}) with a decrease in current density of approximately 92% after 1 h operation at 1.35 *vs.* NHE.[16]

Controlled potential electrolysis with FTO|**1** in a pH neutral P_i solution (0.1 M) allowed us to determine the Faradaic yield of electrocatalytic O_2 evolution. After 1 h and at a potential of 1.35 V *vs.* NHE, a charge of 4.07 C was passed through FTO|**1** and 9.4 μmol of O_2 were detected with a fluorescence oxygen probe (Fig. S3, ESI‡). The O_2 measurement confirms that the anodic catalytic current arises from O_2 evolution with a Faradic efficiency of approximately 90%.

Our electrochemical study suggests that the Co-containing electrocatalyst formed is comparable with the Co–P_i catalyst reported by Nocera's group.[6a,9] The nanocages **1** and **2** show a comparable activity, indicating that the same water oxidation catalyst is formed from these two nanocage precursors on the FTO substrate. Catalytic activity with high stability is only observed in the presence of cobalt ions, and P_i allows for the *in situ* formation of the catalyst from the decomposed TiCo cages under anodic condition.

However, several differences between FTO|TiCo and Co–P_i exist. Scanning electron microscopy (SEM) images of FTO|**1** and FTO|**2** are shown in Fig. 3 and Fig. S4 (ESI‡), respectively. Both electrodes show a similar surface morphology with porous islands and cracks between these islands. For comparison, electrodeposited Co–P_i forms a thin film coalesced with individual 1–5 μm spherical nodule particles.[6a] The porous islands and cracks on FTO|TiCo give access to a high surface area and are presumably formed during the rapid evaporation of dichloromethane. No obvious change is observed in the surface morphology of the islands before and after 1 h applied potential at 1.35 V *vs.* NHE (FTO|**1***). However, electrodeposition of a new layer is observed in the crack area in FTO|**1*** (Fig. 3b).

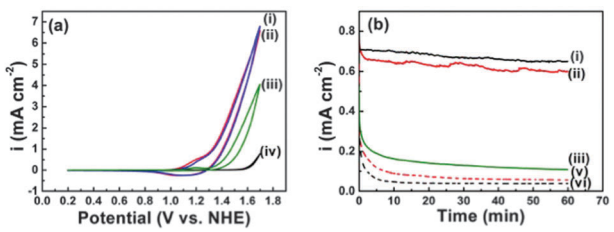

Fig. 2 Electrochemical responses of (i) the FTO|**2**, (ii) the FTO|**1**, (iii) the FTO|-$Co(NO_3)_2$, and (iv) the unmodified FTO electrodes were recorded in an aqueous P_i buffer (0.1 M, solid traces), whereas (v) FTO|**1** and (vi) FTO|**2** were recorded in Na_2SO_4 (0.1 M, dashed traces) at pH 7 and 25 °C. (a) CVs were recorded at a scan rate of 50 mV s^{-1} and (b) chrono-amperometric measurements at 1.35 V *vs.* NHE. The fluctuations in the *i*–*t* curve resulted from the disturbance of O_2 bubbles formed on the surface.

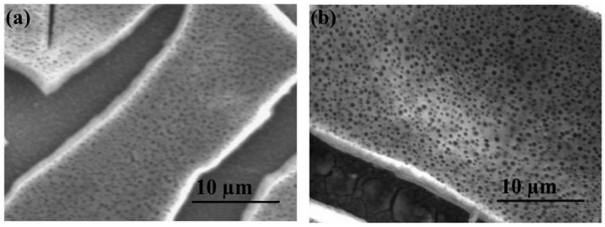

Fig. 3 Planar view SEM images of (a) the as-prepared FTO|**1** and (b) the FTO|**1***.

Table 1 Summary of the EDX analyses of the as-prepared FTO|**1** and the FTO|**1***

	Element content (%)							
Electrode (position)	C	O	Sn	Ti	Co	Br	P	K
FTO|**1** (island)	5.76	56.59	0.00	21.67	5.81	10.18	0.00	0.00
FTO|**1** (crack)	4.03	71.91	21.82	0.71	0.00	0.38	0.00	0.00
FTO|**1*** (island)	0.00	66.73	0.00	14.57	1.15	0.00	9.00	8.56
FTO|**1*** (crack)	0.00	76.38	7.07	0.31	8.24	0.00	4.81	3.19

Detailed examination of the chemical composition of the islands and cracks was carried out by energy dispersive X-ray (EDX) analysis on FTO|**1** (Fig. S5 (ESI‡) and Table 1). Before electrochemical treatment, the Co/Ti ratio of 0.26 in the islands reflects the ratio of these elements in nanocage **1** of 0.22. Co and P are not detectable in the crack area of the FTO|TiCo electrodes before electrochemical treatment. After applying 1.35 V *vs.* NHE for 1 h, the Co content on the islands decreased and significant amounts of Co (8.2%) and P (4.8%) were found on the electro-deposited layers in the crack area. EDX analysis therefore confirms that Co ions migrate under anodic conditions from the islands to the crack area; in analogy to the mechanism suggested for self-healing in Co–P_i.[9] The stoichiometric ratio of Co : P of 2 : 1 in the cracks is also indicative of the formation of a Co–P_i type species.[6a] Powder X-ray diffraction (XRD) studies reveal that the deposited CoO_x catalyst and the titania matrix are amorphous (Fig. S6, ESI‡).

In summary, our study demonstrates that TiCo cages are excellent single-source precursors for the assembly of technologically important materials for water oxidation. By simple drop-casting TiCo cages **1** and **2** on FTO electrodes, we incorporated Co ions in a titania matrix, which form an active CoO_x species *in situ* within minutes by applying a positive potential (>1.2 V *vs.* NHE). Work is currently in progress to study nanosized cages for different redox reactions.

Financial support from EPSRC (EP/H00338X/2) and the Christian Doppler Research Association (Austrian Federal Ministry of Economy, Family and Youth and National Foundation for Research, Technology and Development) and the OMV Group (all to E.R.) is gratefully acknowledged. We also thank the National Science Council of Taiwan (101-2917-I-564-013 to C.Y.L.), a Government scholarship to Study Abroad by the Ministry of Education of Taiwan (SAS-100-1-13-2-UK-034) and the Cambridge Trust (both to Y.H.L.). Y.L. acknowledges support from the China Scholarship Council and the National Natural Science Foundation of China (NSFC 20973127). T.K. was supported by EPSRC. We also thank Mr. Torsten Roth for his help with the synthetic part of the work.

Notes and references

§ *Synthesis of* **2**: CoI_2 (356 mg, 1.14 mmol), $Ti(O^iPr)_4$ (2.0 mL, 9.54 mmol) and ^{i}PrOH (5 mL) were mixed under N_2 in a sample vial and heated in an autoclave at 150 °C for 3 days. Slow cooling to room temperature produced cubic, blue crystals of **2** (600 mg, 27%). ^{1}H NMR spectroscopy shows that **2** is paramagnetic. Direct (allowed) band gap (CH_2Cl_2): 4.68 ± 0.12 eV; indirect (forbidden) band gap (CH_2Cl_2): 3.35 ± 0.05 eV (see Fig. S1, ESI‡). [a]E_p = 1.0 V *vs.* NHE (CH_2Cl_2/[Bu_4N][BF_4]; see Fig. S2, ESI‡). The synthetic procedure and characterisation for **1** can be found in ref. 14.

¶ *Crystal data for* **2**: $[(CoI)Ti_{11}O_{14}(O^iPr)_{17}]\cdot(^iPrOH)_{0.5}$ ($C_{52.5}H_{123}CoIO_{31.5}Ti_{11}$), M_r = 1971.24, monoclinic, space group P_n, Z = 2, a = 14.917(6), b = 13.821(5), c = 20.851(8) Å, β = 90.191(7)°, V = 4299(3) Å^3, μ(Mo–K_α) = 1.523 mm^{-1}, ρ_{calc} = 1.577 g cm^{-3}, T = 100(2) K. Total reflections 19 194, unique 7985 (R_{int} = 0.127). R_1 = 0.075 [$I > 2\sigma(I)$] and wR_2 = 0.225 (all data). The crystal was mounted on a glass fibre with oil (in order to protect it from atmospheric moisture in particular). Data were collected on a Bruker Smart Apex diffractometer. The crystals diffracted only weakly, therefore the data were truncated at a resolution of d < 1.00 Å. The structure was refined by full-matrix least squares on F^2.[17] Co, Ti and I atoms were refined anisotropically, C and O atoms isotropically. H-atoms were constrained in geometrically ideal positions for methylene and methyl groups, respectively.

1 (*a*) A. J. Bard and M. A. Fox, *Acc. Chem. Res.*, 1995, **28**, 141–145; (*b*) O. Khaselev and J. A. Turner, *Science*, 1998, **280**, 425–427; (*c*) S. Y. Reece, J. A. Hamel, K. Sung, T. D. Jarvi, A. J. Esswein, J. J. H. Pijpers and D. G. Nocera, *Science*, 2011, **334**, 645–648.
2 (*a*) T. A. Betley, Q. Wu, T. Van Voorhis and D. G. Nocera, *Inorg. Chem.*, 2008, **47**, 1849–1861; (*b*) R. I. Cukier and D. G. Nocera, *Annu. Rev. Phys. Chem.*, 1998, **49**, 337–369; (*c*) M. H. V. Huynh and T. J. Meyer, *Chem. Rev.*, 2007, **107**, 5004–5064.
3 (*a*) M. Hara, C. C. Waraksa, J. T. Lean, B. A. Lewis and T. E. Mallouk, *J. Phys. Chem. A*, 2000, **104**, 5275–5280; (*b*) A. Harriman, I. J. Pickering, J. M. Thomas and P. A. Christensen, *J. Chem. Soc., Faraday Trans.*, 1988, **84**, 2795–2806.
4 (*a*) M. Kato, T. Cardona, A. W. Rutherford and E. Reisner, *J. Am. Chem. Soc.*, 2012, **134**, 8332–8335; (*b*) A. Badura, B. Esper, K. Ataka, C. Grunwald, C. Wöll, J. Kuhlmann, J. Heberle and M. Rögner, *Photochem. Photobiol.*, 2006, **82**, 1385–1390.
5 (*a*) F. M. Toma, A. Sartorel, M. Iurlo, M. Carraro, P. Parisse, C. Maccato, S. Rapino, B. R. Gonzalez, H. Amenitsch, T. Da Ros, L. Casalis, A. Goldoni, M. Marcaccio, G. Scorrano, G. Scoles, F. Paolucci, M. Prato and M. Bonchio, *Nat. Chem.*, 2010, **2**, 826–831; (*b*) R. Liu, Y. Lin, L.-Y. Chou, S. W. Sheehan, W. He, F. Zhang, H. J. M. Hou and D. Wang, *Angew. Chem., Int. Ed.*, 2011, **50**, 499–502; (*c*) F. Li, B. Zhang, X. Li, Y. Jiang, L. Chen, Y. Li and L. Sun, *Angew. Chem., Int. Ed.*, 2011, **50**, 12276–12279.
6 (*a*) M. W. Kanan and D. G. Nocera, *Science*, 2008, **321**, 1072–1075; (*b*) S. D. Tilley, M. Cornuz, K. Sivula and M. Grätzel, *Angew. Chem., Int. Ed.*, 2010, **49**, 6405–6408; (*c*) T. Takashima, K. Hashimoto and R. Nakamura, *J. Am. Chem. Soc.*, 2012, **134**, 1519–1527; (*d*) M. Yagi, E. Tomita, S. Sakita, T. Kuwabara and K. Nagai, *J. Phys. Chem. B*, 2005, **109**, 21489–21491.
7 V. Artero, M. Chavarot-Kerlidou and M. Fontecave, *Angew. Chem., Int. Ed.*, 2011, **50**, 7238–7266.
8 J. A. Seabold and K.-S. Choi, *Chem. Mater.*, 2011, **23**, 1105–1112.
9 D. A. Lutterman, Y. Surendranath and D. G. Nocera, *J. Am. Chem. Soc.*, 2009, **131**, 3838–3839.
10 Q. Yin, J. M. Tan, C. Besson, Y. V. Geletii, D. G. Musaev, A. E. Kuznetsov, Z. Luo, K. I. Hardcastle and C. L. Hill, *Science*, 2010, **328**, 342–345.
11 J. J. Stracke and R. G. Finke, *J. Am. Chem. Soc.*, 2011, **133**, 14872–14875.
12 (*a*) S. Eslava, F. Hengesbach, M. McPartlin and D. S. Wright, *Chem. Commun.*, 2010, **46**, 4701–4703; (*b*) S. Eslava, M. McPartlin, R. I. Thomson, J. M. Rawson and D. S. Wright, *Inorg. Chem.*, 2010, **49**, 11532–11540; (*c*) S. Mishra, E. Jeanneau, M.-H. Berger, J.-F. Hochepied and S. Daniele, *Inorg. Chem.*, 2010, **49**, 11184–11189.
13 (*a*) M. Dan-Hardi, C. Serre, T. Frot, L. Rozes, G. Maurin, C. Sanchez and G. Férey, *J. Am. Chem. Soc.*, 2009, **131**, 10857–10859; (*b*) R. C. Snoebergerrd, 3rd, K. J. Young, J. Tang, L. J. Allen, R. H. Crabtree, G. W. Brudvig, P. Coppens, V. S. Batista and J. B. Benedict, *J. Am. Chem. Soc.*, 2012, **134**, 8911–8917.
14 Y. Lv, J. Willkomm, A. Steiner, L. Gan, E. Reisner and D. S. Wright, *Chem. Sci.*, 2012, **3**, 2470–2473.
15 H.-S. Chen and R. V. Kumar, *RSC Adv.*, 2012, **2**, 2294–2301.
16 Annealing FTO|TiCo electrodes at 450 °C had an adverse effect on the electrocatalytic activity (Fig. S7, ESI‡).
17 G. M. Sheldrick, *Acta Crystallogr.*, 2008, **A64**, 112–122.